IEEE Access
Multidisciplinary | Rapid Review | Open Access Journal

Received March 12, 2020, accepted March 18, 2020, date of publication March 30, 2020, date of current version April 15, 2020.

Digital Object Identifier 10.1109/ACCESS.2020.2984170

Highly Efficient Spatially Offset Raman Spectroscopy to Profile Molecular Composition in Bone

HAN CUI, ANDREW GLIDLE, AND JONATHAN M. COOPER
Division of Biomedical Engineering, James Watt School of Engineering, University of Glasgow, Glasgow G12 8LT, U.K.

Corresponding author: Jonathan M. Cooper (jon.cooper@glasgow.ac.uk)

This work was supported by the Engineering and Physical Sciences Research Council (EPSRC) under Grant EP/P001114/1.

ABSTRACT Spatially offset Raman spectroscopy (SORS) offers the prospect of collecting spectral information detailing the molecular composition of biomaterials at greater depths below the surface layers than are normally probed by conventional Raman spectroscopy. By collecting off-axial scattered light, the technique overcomes the large background from in-line light within scattering media. In this paper we present a configuration which enables the highly efficient collection of spectral markers, indicative of bone health, including Raman signatures to assess phosphate, collagen and carbonate content, at millimeter depths. We demonstrate the effectiveness of the technique by performing spectral decompositions to analyze the molecular distribution of these markers non-invasively, using in vitro model systems, comprising bone and tissue, in situ.

INDEX TERMS Depth profile, high efficiency, spatially offset Raman spectroscopy.

I. INTRODUCTION

Raman spectroscopy has previously been used to provide unique ''fingerprint'' information to determine both sample composition and molecular structure in a wide range of materials [1]. When combined with its features of being a label free, non-invasive and potentially non-destructive technique, these attributes have also made it widely applicable in materials characterization for life sciences, forensic science or archaeological investigations [2]–[5].

More recently, Raman Spectroscopy has also been used in biomedical applications, including the evaluation of bone structure, assessing key markers of health that include for example signatures for phosphate, collagen and carbonate content (where variations in the composition, as a ratio of mineral and organic matrix components provide a proxy for health and disease). Examples of such investigations include measurements of the local heterogeneities in native and engineered cartilage surrounding the bone to evaluate regenerative tissue engineering approaches [6], whilst other studies of different bone diseases [7]–[10] have indicated that the technique can be used as a diagnostic tool. Key Raman markers include the measurement of the width of the phosphate band [11] or the ratio of collagen matrix to mineral (as an indicator for bone density and mineralization, both of which change with age and disease). Similarly, determination of the substitution of carbonate ions for phosphate in bone is known to decrease bone crystallite size and increases the number of defects – and again has been used as a measure of bone health [12]. Furthermore, whilst McCreadie *et al.* demonstrated that the ratio of carbonate to phosphate in osteoporotic bone is higher than that in normal bone [13], others have also discussed the potential of Raman as a tool for the diagnosis of bone diseases [14]–[16].

However, one of the deficiencies of Raman spectroscopy remains its shallow penetration depth, a consequence of both the magnitude of the excitation laser light at a certain depth, and the ability of the microspectroscopy instrumentation to detect the resultant Raman excited photons within an appropriate timescale. Thus, in its normal operational mode, Raman microspectroscopy can only interrogate molecular compositions to depths of several hundred micrometers into opaque or heavily scattering samples, thereby restricting its application for *in vivo* testing.

Spatially offset Raman spectroscopy (SORS) [17] expands the current application of co-axial Raman microscopy due to its deep detection ability, enabling its use in bulk analysis e.g. in quality assurance, security screening, and the biomedical

The associate editor coordinating the review of this manuscript and approving it for publication was Henry Hess.

in vivo detection [18]–[21]. It has already been proposed as a method with the potential for in-situ transcutaneous characterization of bones (passing through several millimetres of soft tissue in chicken and humans [18]) as well as in exploring osteogenesis imperfecta with a mouse model (where SORS was shown to be more sensitive than conventional Raman spectroscopy [19]). Finally, the technique has also been used to predict bone mineralization and strength [20].

However, despite the potential for use in biomedical sciences, there can be fundamental issues when using the technique, including complex offset control and low efficiency for the collection of off-axial scattered light (both limiting practical aspects such as the throughput of measurements). As a consequence, more recently, variants of SORS such as fiber-based SORS [22], inverse SORS [23] and SERS-SORS [24], have emerged, primarily with the aim of improving its penetration depth. In addition to these methods, digital micro-mirror devices (DMD) have been used to create a patterned array of collection features enabling the off-set to be pre-programmed. In such systems, the mirror elements within the DMD replace the fibers, commonly used in fiber-based SORS, offering the advantage to the user of being able to change the mirror pattern so as to probe different spatial offsets, without the need to physically reposition optical components in the system (which can be cumbersome and time consuming, as in the case of a fiber-based system). In the original implementation of this method [25], a semi-circular pattern consisting of 16 discrete collection points was used as the DMD pattern to collect spectra from model polymeric constructs [25].

Raman spectra are 10^{-6} weaker than Rayleigh scattered light. In addition, SORS spectra that are collected from ''off-axis'' annuli are even weaker than Raman spectra collected axially (or ''in-line''). As a consequence, the highly efficient collection is important for new applications of SORS, particularly those where sensitive measurements are being made in opaque and highly-scattering media. We now propose an implementation of SORS with both a greater collection efficiency and flexible offset settings, achieved by placing a continuous 'offset' pattern on the DMD. This enables a combination of the highly efficient collection of signals coupled with a greater flexibility in the offset setting. Using chicken bones as exsanguinated hard and soft tissue model samples, we show the ability to reproducibly measure the relationship between spatial offset value and the penetration depth. Further by testing molecular compositions we are able to perform deconvolution of the spectra to show the characterization of key molecular markers at penetration depths of $\sim$2 mm, revealing differences of mineral and organic matrix components in tissues, i.e. providing information for use in a potential diagnostic tool for early-stage disease.

II. MATERIAL AND METHODS

A. SPATIALLY OFFSET RAMAN SYSTEM

In contrast to conventional co-axial Raman spectroscopy, SORS acquires signals from photons that exit the sample from positions that are not on the central axis of the illuminating light i.e. there is a lateral offset between the laser beam and the collected Raman signal, where the latter is due to different lateral migrations of Raman photons in different layers; in contrast, the offset between the source and signal positions in conventional Raman is zero.

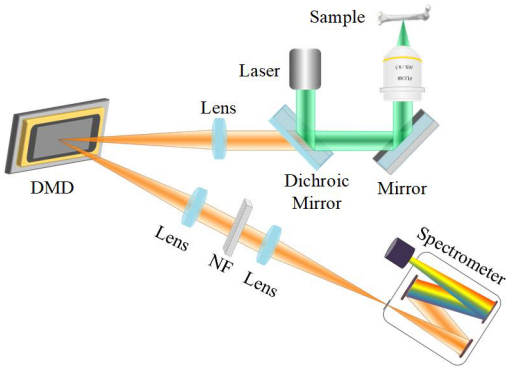

FIGURE 1. Schematic of SORS system with DMD controlling. Note: DMD, digital micro-mirror device; NF, notch filter.

A schematic of the system constructed here is shown in Fig. 1 in which a 532 nm continuous wave (CW) laser (Melles Griot, US) is used as the excitation source (6.8 mW at the sample), which is reflected by a dichroic mirror (DMLP550R, Thorlabs, US) and focused onto the sample after passing through an objective (different objectives used in different tests, 10x, 0.5 NA, Zeiss, Germany, 4x, 0.1 NA, Zeiss, Germany and 2x, 0.06 NA, Olympus, Japan). The SORS signal was collected by the same objective along the original light path, transmitted through the dichroic mirror and focused on a DMD (DLP4500, Texas Instruments, consisting of a 912 x 1140 array of micro-mirrors on a 10.8 μm pitch) by a lens with 125 nm focal length, the pattern of switched on mirrors on the DMD was formed by sending a suitable bit mask to the DLP4500 chip using the control software from Texas Instruments, more detail concerning the relationship between the offset and DMD pattern can be found in [25]. According to the pattern set on the DMD, specific offset Raman signals were reflected and focused into the spectrometer (1200 g/mm grating, Synapse CCD, TRIAX 320, Horiba, France). The spot sizes of the focused laser when using the 10x, 4x and 2x objectives were estimated as 7 μm, 17 μm and 37 μm respectively, and so, as with other SORS measurements, is small compared to the range of offsets measured below.

B. DATA PROCESSING AND MATERIALS

All spectra were processed by Matlab software (version 2017b, The MathWorks, USA) and Origin software (version 2016, OriginLab Corporation., USA) for spectra separation, baseline correction and smoothing. Custom written software was constructed based on Matlab to extract the SORS spectra from the detector image by employing a correction to compensate for 'shifts' in the spectra depending on their vertical

position on the detector. For pre-processing, a polynomial function was used to perform baseline correction by eliminating the fluorescent background and performing Savitzky-Golay smoothing with a two-degree polynomial. For spectra decomposition, multivariate curve resolution was employed to reconstruct the spectra.

The efficiency of the system was first characterized using poly (methyl methacrylate), PMMA sheets, of 3 mm thickness from Oroglas (Arkema Group, France). Chicken bone and its supporting tissue were stored at −18° and defrosted and placed in water immediately prior to measurements. Subsequently, chicken bones were used as exsanguinated hard and soft tissue model samples in order to characterize the instrument's performance in an *in vivo*-like model.

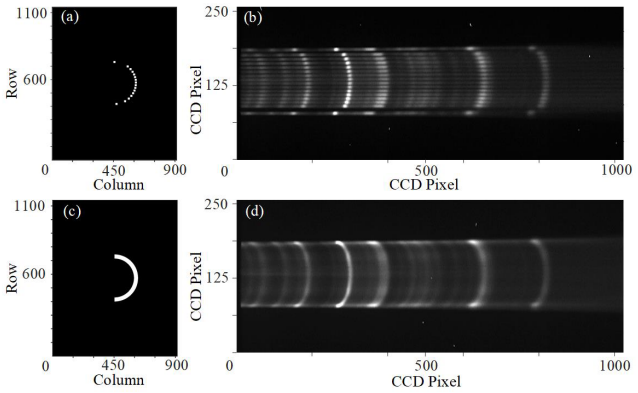

FIGURE 2. Illustration of the mirror pattern used in the discrete (a) and continuous (c) DMD patterns; (b) and (d) images on CCD corresponding to the discrete and continuous patterns. The sample used was a 3 mm thick PMMA sheet. For (a) and (c), the x, y axis are the indices of the micro-mirror array on the DMD chip; for (b) and (d) the x, y axis are CCD pixel elements of the detector.

III. RESULTS AND DISCUSSION

A. HIGHLY EFFICIENT OFFSET RAMAN SIGNAL COLLECTION

As stated, we propose a novel implementation of SORS with a higher efficiency of signal collection and a greater flexibility in the offset settings, achieved by placing a continuous 'offset' pattern within the collection DMD. In contrast to the previous use of discrete DMD patterns for the collection of off-set spectra, as stated, the continuous pattern enables a combination of an improved efficiency of collection of signals with a greater flexibility of the offset setting. To demonstrate the advantages, a comparison between the use of discrete and continuous pattern is shown as Fig. 2. As with other grating spectrometer-based measurements, the spectral resolution was determined by the effective slit width at the entrance to the spectrometer (together with the grating, detector and spectrometer focal length). In the DMD based configuration here, the effective slit width was calculated from the width of the subarray of micro-mirrors that are switched 'on' for a given row in the array (Fig. 2(a)), and the magnifying power of the relay lenses between the DMD array and the spectrometer entrance in this case is around 0.75 (Fig. 1). Thus, a row of 10 switched 'on' micro-mirrors corresponded to an effective slit width of 80 μm.

In order to ensure that the spectra collected on each row of the CCD detector had the same resolution, we kept the number of micro-mirrors that were switched 'on' constant for each row in the DMD array. This had the effect of tapering the width of the annulus formed by the 'on' mirrors, when the width is viewed perpendicular to the annulus normal.

Fig. 2(a) shows a discrete pattern similar to that used previously [25] with the corresponding image on the CCD detector obtained when implemented in our system is shown as Fig. 2(b). Together with the lateral shift of collection points from the centre of the semi-circle pattern on the DMD, the spatial shift of each beam reflected from collection points was collected, giving the spectra shift in different horizontal tracks relative to each other. The gap between each collection point in Fig. 2(a), although not having a significant influence on the average intensity, led to a reduction in the intensity calculated in the 'summed' signal, resulting in a low collection efficiency.

In addition, in practice, some of the emitted Raman light reflected from discrete blocks of switched on DMD mirrors, only partially illuminates the tracks on the CCD due to pixilation effects, leading to difficulties in distinguishing the low-level signals at borders (with the background counts on the detector leading to a degradation in the signal/noise ratio). Thus, when using a discrete pattern, it is difficult to guarantee that every element corresponds to exactly the same offset value with a consequent decrease in both the spatial resolution and reduction in signal to noise quality (i.e. detection limit).

In order to make the system more sensitive, more efficient and more robust, we instead used a continuous semi-circle pattern to acquire the SORS signals, as shown in Fig. 2(c) and (d).

To compare results from the discrete and continuous patterns, we used 16 collection points consisting of 30 × 30 pixels for each of the discrete elements with 10 micro-mirrors forming the vertical gap, as used in a previous study [25]. Fig. 3(a) shows spectra from the continuous and discrete patterns where it can be seen that the collected intensity increases by ∼25% when compared to the former pattern. In the case of both configurations, to obtain the spectra, the locus traced out by a single spectral line (feature) as a function of positional height on the detector can be measured and modelled with a smooth curve (i.e. the locus of a particular bright line in Fig. 2(b) or 2(d)). This model was used to shift the horizontal pixel axis for each of the rows, so that a given spectral feature appears at the same x-pixel number for each row in the transformed detector image.

To validate this approach, we compared the spectra obtained from summing all the rows in an image that result from a continuous DMD pattern, after they have been subjected to such a transformation, with that of a single row in the image. The result shown in Fig. 3(b) illustrate that the spectra from the continuous DMD pattern does not lead to

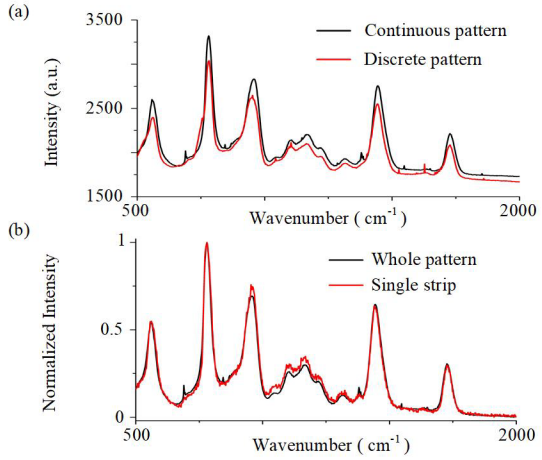

FIGURE 3. (a) Comparison of PMMA spectra detected using discrete and continuous DMD patterns; (b) Comparison of PMMA spectra from the whole continuous pattern and that from a single horizontal strip corresponding to a block of 30 switched on DMD mirrors. The spectra are normalized for clarity.

an increase in the halfwidth in any of the peaks nor is there any crosstalk between rows that leads to a measureable loss in spectral resolution when measuring samples of this type and with this spectrometer grating.

It is important to note that the spectral resolution in the DMD SORS configurations is determined by a convolution of functions involving the width (in the horizontal direction) of the DMD mirror pattern (which corresponds to an effective slit width), the spectrometer grating and the detector. Thus, if highest resolutions are required for samples that have sharp spectral features, the horizontal width at the top and bottom of the arc that defines the continuous DMD pattern should be tapered so as to provide a similar resolution to the central part of the curve.

B. BONE MINERAL COMPOSITION PROFILES

As discussed above, SORS has already been used for the analysis of spectral biomarkers that are proxies of bone health and to date, the DMD-based SORS configuration has been used to characterize either constructs made from thin layers of polymers, or hydroxyapatite mineralization involving polymer scaffolds (with a focus on the polymer and phosphate signals) [25]–[27]. Here, in order to characterize *in vitro* models for bone, we have also focused on measurements that include the relatively weak carbonate signal at 1070 cm^{-1}, a signal that can be masked in systems containing large amounts of polymeric scaffold material. Results have been obtained by either using chicken feet or from model bone-tissue constructs, as illustrated in Fig. 4(a).

SORS spectra presented in Fig. 4(b) were measured at a series of spatial offset values. The top and bottom spectra in the Figure are those of bone and skin alone. It is obvious that the Raman band identified at ~960 cm^{-1} increased from zero to a dominant peak as the spatial offset increased; this band is assigned to $\nu 1(PO_4^{3-})$ of hydroxyapatite [28], [29], the most commonly reported band, characteristic of mineralization.

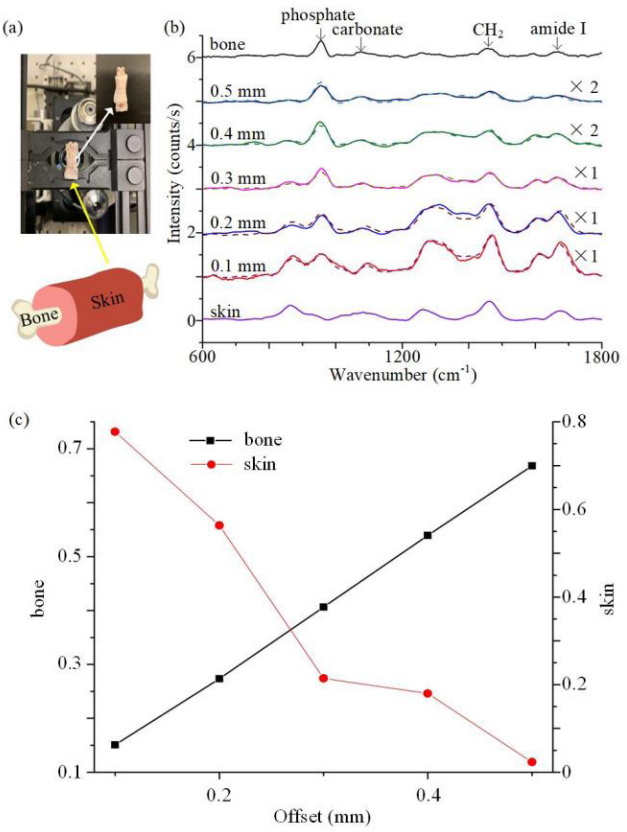

FIGURE 4. (a) Two-layer sample structure consisting of bone and skin; (b) SORS spectra (solid line) recorded at different spatial offset values with the 4x objective, and the reconstructed spectra (dashed line, see also Supplementary Material Supplementary Figure 1) for each offset. (c) The fractional contributions based upon the magnitudes of the reference spectra from skin or bone alone to the reconstructions of (b). Note that the spectra are stacked and scaled for clarity of presentation.

The bands that are the most commonly used for identifying collagen include: the Raman band at ~1450 cm^{-1}, representing $\delta(CH_2)$ deformation; the peak corresponding to the methylene side chains in collagen [11]–[13], [29]; and the peak located at ~1660 cm^{-1} due to the amide I C=O stretch of proteins [30], [31]. Fig. 4(b) shows that the changes in intensity of the collagen bands vary inversely with those of the phosphate band, as the spatial offset value changes. In addition, the peak at ~1070 cm^{-1} from the intense B-type carbonate band $\nu 1$ (CO_3^{2-}) can be used to detect this species [13].

Obtaining the separate component spectra that go to make up the overall measured spectrum for each layer is attractive for further understanding the overall structure of samples probed by SORS. For samples consisting of simple, well segregated, layers where each component has a well defined, simple spectrum, this is easy to accomplish using scaled subtractions to recover the relative contributions of each single component spectrum to the SORS spectra. However, for more complex systems the use of multivariate analyses is more appropriate and tractable. Methods, such as either

multivariate curve resolution (MCR) and/or parallel factor analysis (PARAFAC) can be used to perform this decomposition accurately. Here, we chose the MCR method described previously [32] to perform the spectral decomposition, and obtain the reconstructed spectra shown in Fig. 4(b) as dashed lines for each offset. This used the relative contributions of the skin or bone spectra to construct each SORS spectrum shown as Fig. 4(c), see Supplementary Material Supplementary Figure 1 for the individual skin and bone spectra corresponding to these contributions.

The changes in the relative intensities of the Raman bands as a function of the spatial offset values are shown as Fig. 5. The three different ratios, R(1450 cm^{-1}), R(1660 cm^{-1}) and R(1070 cm^{-1}), were obtained by integrating the area under the peaks at 960 cm^{-1}, 1070cm^{-1}, 1450 cm^{-1} and 1660 cm^{-1} separately, i.e. R(1070 cm^{-1}) = I_{960}/I_{1070}, R(1450 cm^{-1}) = I_{960}/I_{1450} and R(1660 cm^{-1}) = I_{960}/I_{1660}. The results show that all ratios increased as the spatial offset value increases. When the spatial offset value was increased from 0.1 mm to 0.5 mm, the ratios consequently rose from 1.6 to 3.8, 0.5 to 2.2 and 0.3 to 4.5 for R(1070 cm^{-1}), R(1450 cm^{-1}) and R(1660 cm^{-1}) respectively.

The explanation for the increase of these ratios arises from the fact that the offset spectra comprise Raman contributions from both upper and lower layers as well as from Raman photons from deeper layers such as the bone (which have a greater chance to laterally migrate before they escape from the sample at the interface closest to the microscope objective). Therefore, as the spatial offset becomes larger, the contribution to the spectrum from the layers closest to the laser decreases more rapidly than the contribution from the deeper layers [17].

As also discussed above, bone mass reduction is a proxy for osteoporosis. In order to monitor the bone mineral density in bone, the inspection of ratios of mineral to matrix, carbonate to phosphate becomes essential in disease diagnosis and prediction. Relative changes in the mineral to matrix and carbonate to phosphate ratios can be calculated from the measurements here of phosphate (960 cm^{-1}), amide I (1660 cm^{-1}), carbonate (1070 cm^{-1}) and phosphate (960 cm^{-1}), i.e. R (1660 cm^{-1}) and reciprocal of R (1070 cm^{-1}). According to Fig. 5, the carbonate to phosphate ratio decreases due to a smaller contribution from the broad peak around 1000 cm^{-1} - 2000 cm^{-1} from the skin as spatial offset value goes up (this should be considered carefully in any multivariate analysis).

C. DEPTH MEASUREMENTS

Although the high probability of lateral migration of Raman photons emanating from deeper sources in the sample provides a larger detectable depth in SORS, the accessible depth is also affected by the sample's scattering properties. To characterise the penetration depth and assess the feasibility of using the instrument in future in-vivo studies, a series of tests were conducted: Firstly, a chicken limbs were re-constructed as exsanguinated hard and soft tissue models

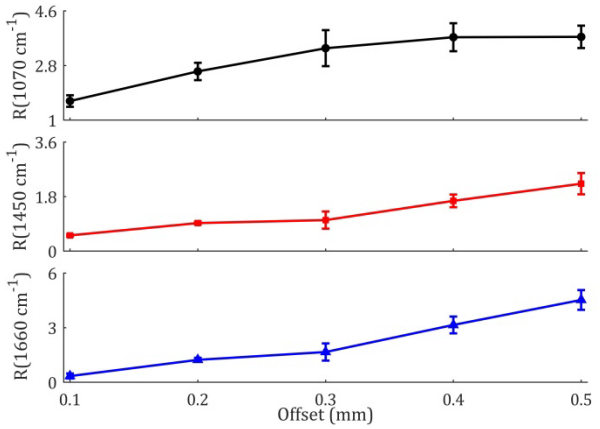

FIGURE 5. Ratios of Raman band intensity corresponding to the peak at 960 cm^{-1} and 1070 cm^{-1} (reciprocal of carbonate to phosphate ratio), 960 cm^{-1} and 1450 cm^{-1}, 960 cm^{-1} and 1660 cm^{-1} (mineral to matrix ratio).

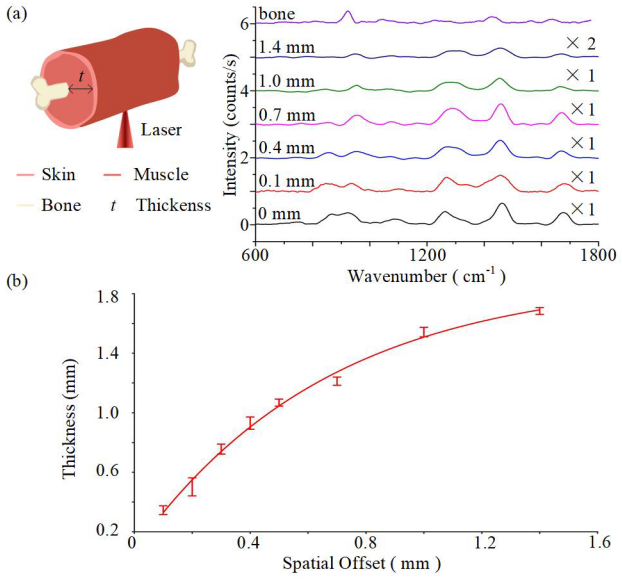

FIGURE 6. (a) Left: Three-layer sample structure consisting of bone, muscle and skin constructed in a sandwich format; Right: an example of SORS spectra recorded at different spatial offset values with the 2x objective for a tissue thickness of 0.93 mm (b) Relation of spatial offset and accessible depth for the 2x objective and DMD array size used. Note that the spectra are stacked and scaled for clarity of presentation.

involving 'sandwiches' comprising fresh chicken skin as the outer layer, muscle tissue as the middle layer and the bone as inner layer were prepared, see Fig. 6(a) left. In these models, the thickness of the tissue layer t was varied. As a method to measure the penetration depth of a given spatial offset distance, we determined the sandwich construct for which the tissue layer thickness that led to the phosphate peak of the bone ceasing to be observable.

Fig. 6(a) right presents the SORS spectra collected for a 0.93 mm thickness middle layer, recorded at various spatial offsets. The CH_2 deformation peaks at 1450 cm^{-1} dominate the spectra, whilst the phosphate peak begins to increasingly

contribute to the acquired spectra at the spatial offsets above 0.4 mm, by presenting an individual peak at 960 cm^{-1}. This peak is likely to be due to more Raman photons migrating further away from the centre of the illumination axis before leaving the sample, where they are collected at a larger offset position. Note, the contribution from the soft tissue layers (skin and muscle) can still be seen when the offset value is above 1 mm but the contribution of the bone spectrum is relatively weak (c.f. Fig. 4).

Fig. 6(b) illustrates the effective spatial offset for which a detectable phosphate signal could be obtained from a given thickness of 'sandwich'. Note, to construct this graph, several different thickness sandwich samples from 0.35 mm to 1.8 mm were measured and measurements from offset values from 0.1 mm to 1.4 mm were made for each one. Analysis of all the spectra showed that, as the thickness increased, the spatial offset value required to get to a detectable boundary (i.e. the phosphate in the bone) must be progressively increased, which is in complete accord with the theory [17]. Thus, for the configuration and 2x objective and DMD array used here, the maximum penetration depth that could be reached in this chicken foot model was 1.7 mm.

IV. CONCLUSION

In summary, a highly efficient, flexible offset SORS system has been demonstrated with the ability to collect molecular profiling data from chicken, as an *in vitro*-like model. By measuring different thicknesses of samples within bone models, a preliminary relationship between spatial offset and penetration depth is provided. A maximum penetration depth using a 2x objective of 1.7 mm was obtained, sufficient to enable the cross-sectional sampling of the long bones of many small animals currently used as models. In addition, novel *in vitro* measurements showing changes in the ratios of mineral to collagen matrix and carbonate to phosphate from the bones are presented, demonstrating the potential of the instrument to provide a non-invasive, rapid, label-free spectroscopic technique to assess biomarkers for the diagnosis of osteoporosis and bone mineralization.

REFERENCES

[1] C. V. Raman and K. S. Krishnan, "A new type of secondary radiation," *Nature*, vol. 121, no. 3048, pp. 501–502, Mar. 1928.

[2] G. S. N. Eliel, M. V. O. Moutinho, A. C. Gadelha, A. Righi, L. C. Campos, H. B. Ribeiro, P.-W. Chiu, K. Watanabe, T. Taniguchi, P. Puech, M. Paillet, T. Michel, P. Venezuela, and M. A. Pimenta, "Intralayer and interlayer electron-phonon interactions in twisted graphene heterostructures," *Nature Commun.*, vol. 9, no. 1, p. 1221, Dec. 2018.

[3] M. Jermyn, K. Mok, J. Mercier, J. Desroches, J. Pichette, K. Saint-Arnaud, L. Bernstein, M.-C. Guiot, K. Petrecca, and F. Leblond, "Intraoperative brain cancer detection with Raman spectroscopy in humans," *Sci. Transl. Med.*, vol. 7, no. 274, p. 274ra19, Feb. 2015.

[4] E. Mistek, L. Halámková, K. C. Doty, C. K. Muro, and I. K. Lednev, "Race differentiation by Raman spectroscopy of a bloodstain for forensic purposes," *Anal. Chem.*, vol. 88, no. 15, pp. 7453–7456, Aug. 2016.

[5] B. Doherty, W. Nowik, C. Miliani, and C. Clementi, "Tyrian purple in archaeological textiles: DMF extraction and recrystallization for the Raman identification of precursors and derivatives," *J. Raman Spectrosc.*, vol. 48, no. 5, pp. 744–749, May 2017.

[6] M. B. Albro, M. S. Bergholt, J. P. St-Pierre, A. V. Guitart, H. M. Zlotnick, E. G. Evita, and M. M. Stevens, "Raman spectroscopic imaging for quantification of depth-dependent and local heterogeneities in native and engineered cartilage," *NPJ Regenerative Med.*, vol. 3, no. 1, Dec. 2018.

[7] M. Khalid, T. Bora, A. A. Ghaithi, S. Thukral, and J. Dutta, "Raman spectroscopy detects changes in bone mineral quality and collagen cross-linkage in staphylococcus infected human bone," *Sci. Rep.*, vol. 8, no. 1, p. 9417, Dec. 2018.

[8] B. Busse, H. A. Bale, E. A. Zimmermann, B. Panganiban, H. D. Barth, A. Carriero, E. Vettorazzi, J. Zustin, M. Hahn, J. W. Ager, K. Püschel, M. Amling, and R. O. Ritchie, "Vitamin d deficiency induces early signs of aging in human bone, increasing the risk of fracture," *Sci. Transl. Med.*, vol. 5, no. 193, p. 193ra88, Jul. 2013.

[9] L. Imbert, J.-C. Aurégan, K. Pernelle, and T. Hoc, "Mechanical and mineral properties of osteogenesis imperfecta human bones at the tissue level," *Bone*, vol. 65, pp. 18–24, Aug. 2014.

[10] T. Pascart, G. Falgayrac, H. Migaud, J.-F. Quinchon, L. Norberciak, J.-F. Budzik, J. Paccou, A. Cotten, G. Penel, and B. Cortet, "Region specific Raman spectroscopy analysis of the femoral head reveals that trabecular bone is unlikely to contribute to non-traumatic osteonecrosis," *Sci. Rep.*, vol. 7, no. 1, p. 97, Dec. 2017.

[11] M. D. Morris and G. S. Mandair, "Raman assessment of bone quality," *Clin. Orthopaedics Rel. Res.*, vol. 469, no. 8, pp. 2160–2169, Aug. 2011.

[12] J. A. Inzana, J. R. Maher, M. Takahata, E. M. Schwarz, A. J. Berger, and H. A. Awad, "Bone fragility beyond strength and mineral density: Raman spectroscopy predicts femoral fracture toughness in a murine model of rheumatoid arthritis," *J. Biomech.*, vol. 46, no. 4, pp. 723–730, Feb. 2013.

[13] B. R. McCreadie, M. D. Morris, T.-C. Chen, D. Sudhaker Rao, W. F. Finney, E. Widjaja, and S. A. Goldstein, "Bone tissue compositional differences in women with and without osteoporotic fracture," *Bone*, vol. 39, no. 6, pp. 1190–1195, Dec. 2006.

[14] G. S. Mandair and M. D. Morris, "Contributions of Raman spectroscopy to the understanding of bone strength," *BoneKEy Rep.*, vol. 4, p. 620, Jan. 2015.

[15] Y. Ishimaru, Y. Oshima, Y. Imai, T. Iimura, S. Takanezawa, K. Hino, and H. Miura, "Raman spectroscopic analysis to detect reduced bone quality after sciatic neurectomy in mice," *Molecules*, vol. 23, no. 12, p. 3081, 2018.

[16] S. R. Goodyear and R. M. Aspden, "Raman microscopy and bone," in *Bone Research Protocols*. New York, NY, USA: Humana Press, 2019, pp. 651–659. Accessed: Feb. 8, 2019. [Online]. Available: https://link.springer.com/content/pdf/10.1007%2F978-1-4939-8997-3.pdf

[17] P. Matousek, I. P. Clark, E. R. C. Draper, M. D. Morris, A. E. Goodship, N. Everall, M. Towrie, W. F. Finney, and A. W. Parker, "Subsurface probing in diffusely scattering media using spatially offset Raman spectroscopy," *Appl. Spectrosc.*, vol. 59, no. 4, pp. 393–400, Apr. 2005.

[18] M. V. Schulmerich, W. F. Finney, V. Popescu, M. D. Morris, T. M. Vanasse, and S. A. Goldstein, "Transcutaneous Raman spectroscopy of bone tissue using a non-confocal fiber optic array probe," *Proc. SPIE*, vol. 6093, Feb. 2006, Art. no. 60930O.

[19] G. Feng, M. Ochoa, J. R. Maher, H. A. Awad, and A. J. Berger, "Sensitivity of spatially offset Raman spectroscopy (SORS) to subcortical bone tissue," *J. Biophotonics*, vol. 10, no. 8, pp. 990–996, Aug. 2017.

[20] C. Shu, K. Chen, M. Lynch, J. R. Maher, H. A. Awad, and A. J. Berger, "Spatially offset Raman spectroscopy for *in vivo* bone strength prediction," *Biomed. Opt. Exp.*, vol. 9, no. 10, p. 4781, Oct. 2018.

[21] M. V. Schulmerich, J. H. Cole, J. M. Kreider, F. Esmonde-White, K. A. Dooley, S. A. Goldstein, and M. D. Morris, "Transcutaneous Raman spectroscopy of murine bone *in vivo*," *Appl. Spectrosc.*, vol. 63, no. 3, pp. 286–295, Mar. 2009.

[22] M. V. Schulmerich, W. F. Finney, R. A. Fredricks, and M. D. Morris, "Subsurface Raman spectroscopy and mapping using a globally illuminated non-confocal fiber-optic array probe in the presence of Raman photon migration," *Appl. Spectrosc.*, vol. 60, no. 2, pp. 109–114, Feb. 2006.

[23] P. Matousek, "Inverse spatially offset Raman spectroscopy for deep non-invasive probing of turbid media," *Appl. Spectrosc.*, vol. 60, no. 11, pp. 1341–1347, Nov. 2006.

[24] N. Stone, K. Faulds, D. Graham, and P. Matousek, "Prospects of deep Raman spectroscopy for noninvasive detection of conjugated surface enhanced resonance Raman scattering nanoparticles buried within 25 mm of mammalian tissue," *Anal. Chem.*, vol. 82, no. 10, pp. 3969–3973, May 2010.

[25] Z. Liao, F. Sinjab, G. Gibson, M. Padgett, and I. Notingher, "DMD-based software-configurable spatially-offset Raman spectroscopy for spectral depth-profiling of optically turbid samples," *Opt. Express*, vol. 24, no. 12, pp. 12701–12712, Jun. 2016.
[26] Z. Liao, F. Sinjab, A. Nommeots-Nomm, J. Jones, L. Ruiz-Cantu, J. Yang, F. Rose, and I. Notingher, "Feasibility of spatially offset Raman spectroscopy for in vitro and *in vivo* monitoring mineralization of bone tissue engineering scaffolds," *Anal. Chem.*, vol. 89, no. 1, pp. 847–853, Jan. 2017.
[27] M. Dooley, A. Prasopthum, Z. Liao, F. Sinjab, J. McLaren, F. R. A. J. Rose, J. Yang, and I. Notingher, "Spatially-offset Raman spectroscopy for monitoring mineralization of bone tissue engineering scaffolds: Feasibility study based on phantom samples," *Biomed. Opt. Express*, vol. 10, no. 4, pp. 1678–1690, Apr. 2019.
[28] M. S. Bergholt, J.-P. St-Pierre, G. S. Offeddu, P. A. Parmar, M. B. Albro, J. L. Puetzer, M. L. Oyen, and M. M. Stevens, "Raman spectroscopy reveals new insights into the zonal organization of native and tissue-engineered articular cartilage," *ACS Cent. Sci.*, vol. 2, no. 12, pp. 885–895, Nov. 2016.
[29] G. Penel, C. Delfosse, M. Descamps, and G. Leroy, "Composition of bone and apatitic biomaterials as revealed by intravital Raman microspectroscopy," *Bone*, vol. 36, no. 5, pp. 893–901, May 2005.
[30] Z. Huang, S. K. Teh, W. Zheng, K. Lin, K. Y. Ho, M. Teh, and K. G. Yeoh, "*in vivo* detection of epithelial neoplasia in the stomach using image-guided Raman endoscopy," *Biosensors Bioelectron.*, vol. 26, no. 2, pp. 383–389, Oct. 2010.
[31] A. J. Makowski, C. A. Patil, A. Mahadevan-Jansen, and J. S. Nyman, "Polarization control of Raman spectroscopy optimizes the assessment of bone tissue," *J. Biomed. Opt.*, vol. 18, no. 5, May 2013, Art. no. 055005.
[32] K. Buckley, J. G. Kerns, A. W. Parker, A. E. Goodship, and P. Matousek, "Decomposition of *in vivo* spatially offset Raman spectroscopy data using multivariate analysis techniques," *J. Raman Spectrosc.*, vol. 45, no. 2, pp. 188–192, Feb. 2014.

HAN CUI received the Ph.D. degree in instrument science and technology from the Beijing Institute of Technology, China. She is currently an Early-Career Researcher with the Division of Biomedical Engineering, University of Glasgow, U.K. She has published a number of articles in specialist optics journals, as well as being a named inventor on granted patents in the development of confocal microscopy. Her research interests include theory, instrumentation, and experimental measurement for Raman spectroscopy.

ANDREW GLIDLE received the Ph.D. degree in electrochemistry from Exeter University, U.K. He is currently a Senior Research Fellow in biomedical engineering with the University of Glasgow, U.K. Throughout his career he has been extensively involved in interdisciplinary collaborations with research focused on the development of materials for (bio)sensor interfaces and sensing techniques, optical and electronic microsystems, and the design of instrumentation and analytical techniques.

JONATHAN M. COOPER received the Ph.D. degree in biosensor technologies from the University of Cranfield, U.K. He was involved as an Academic Founder of spin-out companies in the fields of medical diagnostics, drug delivery, and new medicines discovery. He has 280 publications in internationally renowned peer-reviewed publications, with an ISI H factor of 52. He was elected as a Fellow of the Royal Society of Edinburgh, in 2001, and the Royal Academy of Engineering, in 2004. He holds The Wolfson Chair in biomedical engineering.